2007 IEEE International Conference on
Robotics and Automation
Roma, Italy, 10-14 April 2007

The Optimum Design of a 6-DOF Parallel Manipulator with Large Orientation Workspace

Yoon-Kwon Hwang, Jung-Won Yoon, Christiand, and Je-Ha Ryu

***Abstract*— An objective of this research is to optimize the designing parameters of a 6-DOF parallel manipulator required the large workspace for the sophisticated and complicated work on the basis of mechanism's compactness. The method uses a genetic algorithm with respect to the maximization of tranlational/rotational workspaces and isotropy of mechanism to obtain the optimal linkage parameters. It is studied for fifteen cases which are divided by combination of translational and rotational workspaces corresponding to the range of translational motion and tilt angle of the end-effector. To decide the best model in the total optimized cases, compactness of mechanism, translational workspace, rotational workspace on the boundary of translational workspace, and global conditioning index (GCI) as kinematic performances, and then kinematic performances of best model are verified by comparing to those of the pre-existing model.**

I. Introduction

Parallel manipulators possess many advantages in comparison with serial manipulators in terms of high stiffness, smaller masses of links, the possibility of carrying bigger loads, as well as higher accuracy. Because of these advantages, the application field of parallel manipulator has been developed and expended with changing the mechanical design such as degree of freedom and/or number of linkages and arrangement of actuator, etc. [1], [2], [3]. The only drawback of them, however, is a smaller workspace. Therefore the main purpose of many researchers have been focused on the techniques to improve mechanism's parameters in order to increase workspace and isotropy of manipulator so far [4], [5], [6], [7].

This paper proposes the optimum design method of a parallel manipulator, which has the pantograph parallel mechanism with compactness and lightness in order to use it as the haptic device for the sophisticated and complicated work required the large rotational workspace such as the assemble task of aerospace parts. The approach is to prepare a few of given translational and rotational workspaces according to the change of circle radius and rotation angle, and then to calculate an objective function maximizing the synthetic value of translational and rotational workspaces and global conditioning index (GCI) throughout the entire given workspaces in optimization process of a genetic algorithm. In this paper, total fifteen types, which are divided by combination of given translational and rotational workspaces, are studied, and each result of them is obtained, and then the best model is selected by comparing to a half size of pre-existing model in [8].

This work was supported by the Korea Research Foundation Grant funded by the Korean Government(MOEHRD) (KRF-2005-005-J09902) and was supported by NURI Project.

Y. K. Hwang is with the Technical Research Institute, Hyundai Mobis Company, Yongin, Korea, ykhwang@mobis.co.kr

J. W. Yoon is with the School of Mechanical and Aerospace Engineering and ReCAPT, Gyeongsang National University, Jinju, Korea jwyoon@gsnu.ac.kr

Christiand is with the School of Mechanical and Aerospace Engineering, Gyeongsang National University, Jinju, Korea tianize@yahoo.com

J. H. Ryu is with the Department of Mechatronics, Gwangju Institute of Science and Technology, Gwangju, Korea ryu@gist.ac.kr

II. Mechanical Description and Kinematic Analysis

The proposed 6-DOF haptic device, as shown in Fig. 1, is basically similar to the parallel mechanism of [8] in terms of having three pantograph mechanisms that are driven by six base-fixed servomotors with the 3-RRR type spherical joints on the top of the pantograph mechanism, an end-effector and the connecting bars.

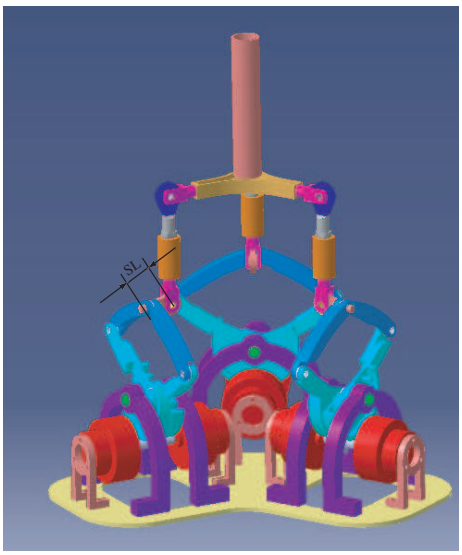

Fig. 1. The proposed 6-DOF haptic device.

To obtain static characteristics of mechanism, kinematic parameters are shown in Fig. 2. The global reference frame, denoted by $\Sigma_b(X_b, Y_b, Z_b)$, is located on center of active joints. The local frames of an end-effector and each pantograph are denoted by $\Sigma_{o'}(X_{o'}, Y_{o'}, Z_{o'})$ and $\Sigma_{pi}(X_{pi}, Y_{pi}, Z_{pi})$ $(i = 1, 2, 3)$, respectively. The axisymmetric positions of each pantograph and revolute joint are given by angles δ_i and γ_i $(i = 0, \frac{2}{3}\pi, \frac{4}{3}\pi)$ with radii of R_0 and R_1 . Each pantograph has 2-DOF motion on the $Y_{pi} - Z_{pi}$ plane. Notice that even though the spherical joints look to be located on the top of pantograph mechanisms, those actual centers are located in an offset distance

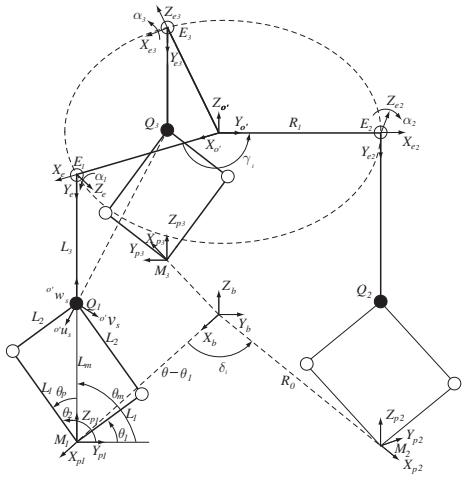

Fig. 2. The kinematic model.

of *SL* (see Fig. 1). In the kinematic analysis, however, center of spherical joint is assumed just on the top of a pantograph mechanism because of the offset distance does not affect its results if R_0 is replaced by $R_{0'} - SL$. Lower and upper links of pantograph and the connecting bar are denoted by L_1, L_2, and L_3. The M_i, Q_i, and E_i present the positions of active, spherical, and revolute joints.

In the calculation of inverse kinematics, the active joint angles θ_{1i} and θ_{2i} of each pantograph are obtained for given position and rotation $(x, y, z, \phi, \theta, \rho)$ of an end-effector. Furthermore, the Jacobian matrix can be easily derived by using the concept of reciprocal screws. More details about them were described in [8].

III. Design requirements

A. Linkage parameter and design variable

The linkage parameters deciding the size of haptic device consist of L_1, L_2, L_3, R_0, R_1, and *SL* (see Fig. 1 and Fig. 2). This RRR type spherical joint, however, does not allow full rotation even though the largest possible rotation and easy installation. Therefore, pre-existing device was developed with considering *SL* to maximize the rotation angle of L_3 for large workspace. Tab. I shows a half values of pre-existing model's parameters which consist of base model for evaluation of optimized model in this research. Here, P_z is an end-effector's neutral position, which takes same amount of displacement: $(0, 0, \pm 40)$ along to the Z axis in Σ_b on the condition of $L_2 = L_1$, $R_1 = R_0 - SL$, $\theta_{1i} = 30^\circ$ and $\theta_{2i} = 120^\circ$, and then it is automatically calculated by L_1, L_3, and R_0. As a result, L_1, L_3, and R_0 are used as variables to calculate an objective function of a genetic algorithm in optimization process.

The higher neutral position of an end-effector, the larger translational workspace. The rotational workspace, however, is not always increase proportionally, because of mechanism's singularity when the pantograph mechanisms are either lowered down to the base plate plane or are vertically erected, or all the connecting bars are perpendicular to pantograph planes. Accordingly, the neutral position $\mathbf{P}(0, 0, P_z)$ in Σ_b should be considered as a factor to evaluate the compactness of haptic device.

TABLE I
Linkage parameters of pre-existing model.

Value of linkage parameter						
P_z	L_1	L_2	L_3	R_0	R_1	SL
240mm	80mm	80mm	160mm	130mm	100mm	30mm

B. Given translational workspace

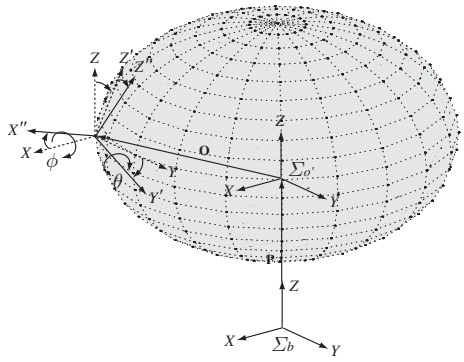

Fig. 3. The given translational workspace.

To implement a genetic algorithm, the translational workspace as the given workspace to evaluate the range of translational motion and isotropy of mechanism must bounded and discretized as shown in Fig. 3. It, denoted by Ω, is uniformly spaced surface as the sphere's form. The Ω consists of a set of N by discretized point n_k, where $k = 1, 2, 3, \cdots, N$. Here, total discretized number is counted by $N(N-1)+2$. The coordinate of n_k is known: $\mathbf{O}_k(X_k, Y_k, Z_k)$ in $\Sigma_{o'}$. A number of points are distributed in Ω, and for each of them, the inverse kinematic problem is solved. If it results in real solutions of the joint variables, the point is said to be belong to Ω. Samples Ω_i are prepared according to change of sphere radius in optimization process using a genetic algorithm.

C. Given rotational workspace

The rotational workspace as another given workspace must also bounded and discretized by the roll-pitch-yaw angles as shown in Fig. 3. The rotational workspace, denoted by Γ, is also uniformly spaced by roll-pitch-yaw angles $\Psi(\phi, \theta, \gamma)$, called tilt angle, where ϕ and θ are bounded and γ is left constrained as $\gamma = 0$. The Γ consists of a set of M by discretized angle m_k, where $k = 1, 2, 3, \cdots, M$. Here, total discretized angle number is counted by $(M+1)^2$. The m_k is generated at $\mathbf{O}_{k_1}(X_k, 0, 0)$, $\mathbf{O}_{k_2}(0, Y_k, 0)$, $\mathbf{O}_{k_3}(0, 0, Z_k)$, and $\mathbf{O}_{k_4}(0, 0, -Z_k)$ which are located on the boundaries along to X, Y, and $\pm Z$ axes in Ω. A number of discretized angles are distributed in Γ, and for each of them, the inverse kinematic problem is solved. If it results in real solutions of the joint

variables, the angle is also said to be belong to Γ. Samples Γ_i are prepared according to change of Ψ_i in optimization process using a genetic algorithm.

IV. Formulation of Optimization

A. Application of genetic algorithm

Most of optimization problems we treat are difficult, because they are not only complicate but also insufficient about reciprocal relationship between variables and *a priori* knowledge for a function. Among them, the genetic algorithm is the probability based on the optimization method describing genetics and natural evolution numerically [9], [10]. The method is based on the creation and evolution of many individuals that, through several generations, become stronger. Each randomly created individual represents a set of mechanism parameters. The strengths of these individuals (L_1,L_3,R_0) are evaluated by an objective function. The evolution of the individuals is accomplished using genetic operators such as selection, crossover, and mutation until the method converges towards an optimal solution. Especially, it is useful to the proposed model of complicated mechanism, because of robustness to search the solution. Tab. II shows parameters used in a genetic algorithm.

TABLE II
Parameters used to a genetic algorithm.

Parameters	
Number of individual in a population	100
Maximum number of generations	50
Probability of crossover	0.85
Probability of mutation	0.05

B. Definition of objective function

From the synthesis of individuals, the object function, denoted by $F(x)$, can be obtained by the form of maximization with positive value in optimization process using a genetic algorithm as follows:

$$F(x) = \text{Max.}\left\{ \frac{n_{\text{in}}}{N_{\text{tot}}} + \sum_{i=1}^{4} \left(\frac{m_{i,\text{in}}}{M_{i,\text{tot}}} \right) + \text{GCI} \right\}, \tag{1}$$

where n_{in}, m_{in} are the number of discretized points and angles, which have fallen into Ω and Γ, and N_{tot}, $M_{i,\text{tot}}$ are the total number of discretized points and angles in optimization process to calculate the real solution by the inverse kinematics.

C. Constraints of system boundary

To calculate an objective function, constraints for system boundaries should be defined through analysis of motion expected in advance. In order to the optimal solution of Eq. (1) in the imposed solution space, initial posture and singularity configuration of mechanism should be considered as well as range of linkage length.

The following parameters are used as the optimal variables: L_1, L_3, and R_0. All other parameters are left constrained as $L_2 = L_1$, $SL = 15$ (see Tab. I), $R_1 = R_0 - SL$, and P_z by L_1 and L_3 at $\theta_{1i} = 30^\circ$ and $\theta_{2i} = 120^\circ$. Accordingly, the constraints of parameters for system boundary are defined as:

$$\Lambda = \{\mathbf{x} | \mathbf{x}^{(L)} \leq \mathbf{x} \leq \mathbf{x}^{(U)}\}, \tag{2}$$

where Λ is the solution space which is composed of real solution for joint variables in the inverse kinematics, and is restricted by the values of lower limited vector $\mathbf{x}^{(L)}$ and upper limited vector $\mathbf{x}^{(U)}$ for $\mathbf{x} = (L_1, L_3, R_0)$. The $\mathbf{x} \in \Lambda$ satisfied all of the imposed constraints is called the feasible solution in the optimization process of a genetic algorithm. Each range is shown in Tab. III. The $\mathbf{x}_{\text{init}}$ is of base model, and each of $\mathbf{x}^{(L)}$ and $\mathbf{x}^{(U)}$ is set corresponding to 60% of base model.

D. Construction of given workspace

In the optimization process to calculate the value of an objective function, the given workspaces are prepared by combination of Ω and Γ. They are divided three types into Ω_i, and then each of them is discriminated by Γ_i with respect to range of translational motion and tilt angle corresponding to the real solution of inverse kinematics as shown in Tab. IV. As a result, the total fifteen given workspaces are constructed: Type I_i $(i = 1 \sim 7)$ by Γ_i $(i = 10, 15, \cdots, 40)$ for Ω_{20}, Type II_i $(i = 1 \sim 5)$ by Γ_i $(i = 10, 15, \cdots, 30)$ for Ω_{30}, and Type III_i $(i = 1 \sim 3)$ by Γ_i $(i = 10, 15, 20)$ for Ω_{40}, respectively.

TABLE IV
Discrete translational and rotational workspaces.

Position				
Ω_i	Axis	Min	Max	N
Ω_{20}	**i**, **j**, **k**	-20mm	20mm	17
Ω_{30}	**i**, **j**, **k**	-30mm	30mm	
Ω_{40}	**i**, **j**, **k**	-40mm	40mm	
Total discrete points			274	

Rotation					
Γ_i	Axis	Min	Max	Step	M
Γ_{10}	**i**,**j**	-10°	10°	1.25°	16
Γ_{15}	**i**,**j**	-15°	15°	1.875°	
Γ_{20}	**i**,**j**	-20°	20°	2.5°	
Γ_{25}	**i**,**j**	-25°	25°	3.125°	
Γ_{30}	**i**,**j**	-30°	30°	3.75°	
Γ_{35}	**i**,**j**	-35°	35°	4.375°	
Γ_{40}	**i**,**j**	-40°	40°	5.0°	
Total discrete angles				289	

V. Results

A. Results of computation

The maximum values of an objective function are decide by converging the values of variables in the optimization process using a genetic algorithm. The total fifteen cases are studied, and then, for each of them, the optimized L_1, L_3, and R_0 are obtained with P_z as shown in Tab. V.

In addition, Tab. VI shows the performance indices based on each optimized parameter (see Tab. V). To evaluate the relative comparison of isotropy for fifteen cases, GCI_i are carried out for Ω_{20}. And Ω_i are also evaluated, and those

TABLE III
RANGE OF CONSTRAINT.

Variables								
L_1			L_3			R_0		
x_{init}	$x^{(U)}$	$x^{(L)}$	x_{init}	$x^{(U)}$	$x^{(L)}$	x_{init}	$x^{(U)}$	$x^{(L)}$
40mm	64mm	16mm	80mm	128mm	32mm	65mm	104mm	26mm

TABLE VI
VALUES OF PERFORMANCE INDICES FOR OPTIMIZED PARAMETERS.

Type	Ω				Γ				GCI
					$\mathbf{P}$		$\mathbf{O}_k$		
	$\pm X$	$\pm Y$	$+Z$	$-Z$	$\Psi_{\max}$	$\Psi_{\min}$	$\Psi_{\max}$	$\Psi_{\min}$	At Ω_{20}
Base	75mm	78mm	40mm	44mm	49.8°	39.3°	25.8°	13.5°	0.0279
Type I_1	81mm	82mm	42mm	47mm	32.7°	27.9°	19.8°	10.5°	0.0526
Type I_2	78mm	89mm	53mm	60mm	41.7°	35.1°	28.5°	17.4°	0.0519
Type I_3	75mm	86mm	62mm	67mm	50.1°	42.0°	36.6°	22.8°	0.0515
Type I_4	64mm	74mm	64mm	71mm	58.8°	51.6°	43.8°	27.3°	0.0423
Type I_5	74mm	85mm	64mm	68mm	64.2°	58.5°	46.5°	33.6°	0.0347
Type I_6	58mm	67mm	63mm	70mm	74.4°	63.0°	56.4°	36.0°	0.0285
Type I_7	49mm	56mm	64mm	67mm	81.3°	62.1°	67.5°	37.8°	0.0249
Type II_1	109mm	103mm	53mm	63mm	35.4°	33.9°	17.7°	7.5°	0.0518
Type II_2	109mm	122mm	62mm	69mm	42.6°	39.9°	25.5°	14.1°	0.0513
Type II_3	77mm	89mm	64mm	68mm	55.2°	54.0°	32.1°	17.1°	0.0404
Type II_4	75mm	86mm	64mm	69mm	71.1°	59.4°	37.2°	20.4°	0.0317
Type II_5	62mm	71mm	64mm	71mm	84.9°	65.4°	43.5°	20.4°	0.0259
Type III_1	120mm	126mm	64mm	71mm	43.8°	38.7°	15.9°	5.7°	0.0512
Type III_2	110mm	126mm	64mm	72mm	59.4°	42.9°	19.2°	6.9°	0.0369
Type III_3	84mm	97mm	64mm	70mm	76.2°	54.6°	21.0°	5.4°	0.0271

TABLE V
VALUES OF OPTIMIZED PARAMETERS BY A GENETIC ALGORITHM.

Type	P_z	L_1	L_3	R_0
Base	120.0mm	40.0mm	80.0mm	65.0mm
Type I_1	129.1mm	41.9mm	87.2mm	104.0mm
Type I_2	136.0mm	52.6mm	83.4mm	104.0mm
Type I_3	142.1mm	62.5mm	79.6mm	104.0mm
Type I_4	132.3mm	64.0mm	68.3mm	89.3mm
Type I_5	142.9mm	64.0mm	78.9mm	77.0mm
Type I_6	125.4mm	63.2mm	62.2mm	67.1mm
Type I_7	116.4mm	64.0mm	52.4mm	61.6mm
Type II_1	170.0mm	52.6mm	117.4mm	104.0mm
Type II_2	179.2mm	62.5mm	116.7mm	104.0mm
Type II_3	146.6mm	64.0mm	82.6mm	86.2mm
Type II_4	143.6mm	64.0mm	79.6mm	72.1mm
Type II_5	130.0mm	64.0mm	66.0mm	62.9mm
Type III_1	192.0mm	64.0mm	128.0mm	104.0mm
Type III_2	182.2mm	64.0mm	118.2mm	80.7mm
Type III_3	154.2mm	64.0mm	90.2mm	64.7mm

ranges for three translational directions are presented at each neutral position $\mathbf{P}_i(0,0,P_{zi})$ of an end-effector, and Γ_i are at $\mathbf{O}_{k,i}(O_{k,xi},O_{k,yi},\pm O_{k,zi})$ on boundaries of Ω_i. From the geometric structure of this mechanism, Γ_i generate larger at $\mathbf{O}_{k,i}(O_{k,xi},O_{k,yi},-O_{k,zi})$ than at $\mathbf{O}_{k,i}(O_{k,xi},O_{k,yi},O_{k,zi})$, so that values of Ψ_i on the boundaries (see Tab. VI) are represented at $\mathbf{O}_{k,i}(O_{k,xi},O_{k,yi},O_{k,zi})$. Here, this representing method of Ψ is based on the use of a modified set of Euler angles and the particular representation of the rotational workspace in a cylindrical coordinate system as this guarantees that the rotational workspace is a single volume [11] as shown in Fig. 4 and Fig. 5. It is defined as the set of possible directions of the approach vector (represented by two tilt angles: ϕ, θ) of an end-effector and finding an intersection of the rotational workspace. The isotropy of mechanism can be evaluated from workspace's configuration with values of $\Psi_{\max}$ and $\Psi_{\min}$. Fig. 4 and Fig. 5 show the projected rotational workspaces of an end-effector at $\mathbf{P}_i$ in Σ_b and at $\mathbf{O}_{k,i}$ in $\Sigma_{o'}$ for all of the cases, respectively.

B. Evaluation of proposed model

In order to compare critically, Fig. 8 shows the volumes of translational workspaces between the base model and the proposed model as the best one. Each range of three translational directions is ± 75, ± 78, 40, -44mm on the base model and ± 74, ± 85, 64, -68mm on the proposed model along to $\pm X$, $\pm Y$, Z, $-Z$ axes in Σ_b. To compare the difference of volumes, the error ratio, denoted by $\mathbf{e}$, becomes -1.3, 9.0, and 57.1%, where for example $e_z = ((\| \pm Z\|_{(b)} - \| \pm Z\|_{(a)})/\| \pm Z\|_{(a)}) \times 100\%$. The proposed model is better than the base model with respect to the two directions. Especially, the difference of them is immensely in Z axis.

Fig. 6 shows the rotational workspaces in cylindrical coordinates: (a), (b), and the projected rotational workspaces: (c) of the base and proposed models at each $\mathbf{P}$ of an end-effector.

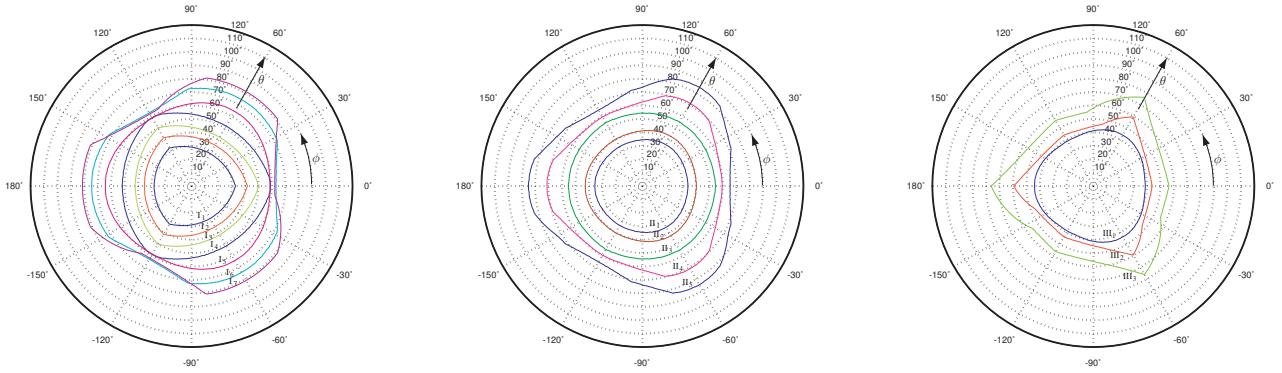

(a) Type I_i (b) Type II_i (c) Type III_i

Fig. 4. Comparison of projected rotational workspace of translational workspace for fifteen cases at each neutral position $\mathbf{P}_i(0,0,P_{zi})$ in Σ_b.

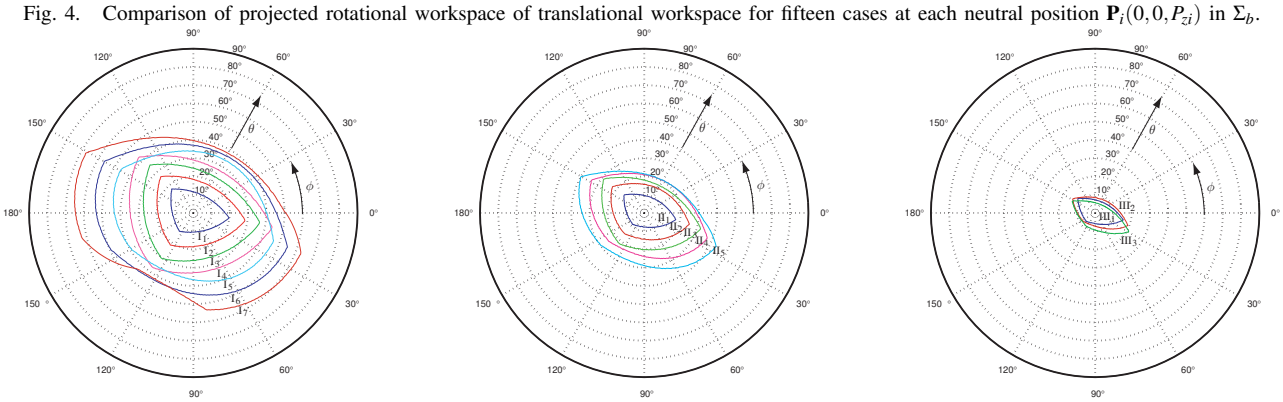

(a) Type I_i (b) Type II_i (c) Type III_i

Fig. 5. Comparison of projected rotational workspace of translational workspace for fifteen cases at each boundary position $\mathbf{O}_k, i(O_{k,xi}, O_{k,yi}, O_{k,zi})$ in $\Sigma_{o'}$.

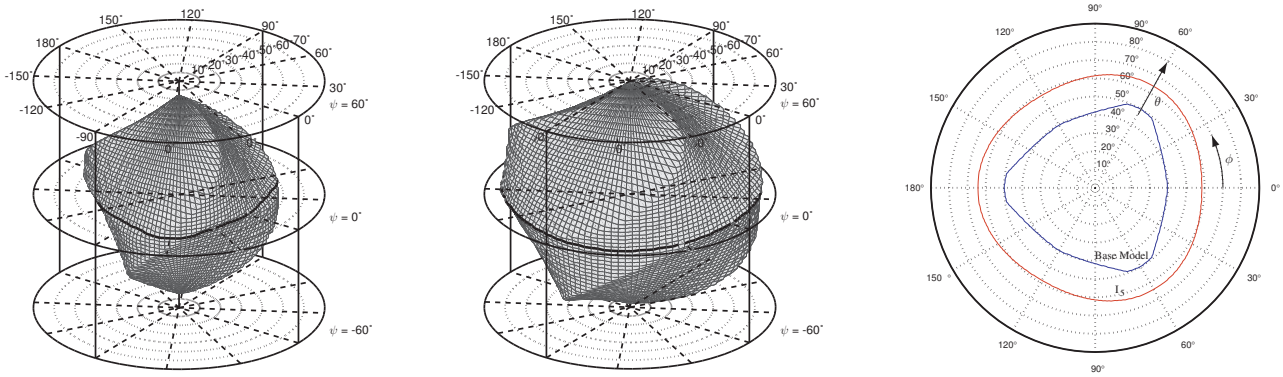

(a) Base model (b) Proposed model (c) Base/proposed models

Fig. 6. Comparison of rotational workspaces in cylindrical coordinates and the projected rotational workspaces at each neutral position ((a): $\mathbf{P}(0,0,120)$, (b): $\mathbf{P}(0,0,142.9)$).

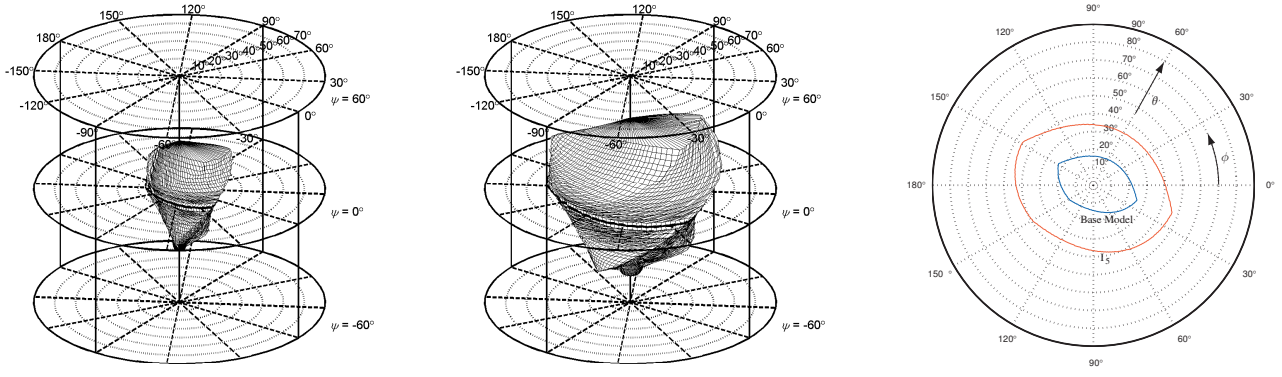

(a) Base model (b) Proposed model (c) Base/proposed models

Fig. 7. Comparison of rotational workspaces in cylindrical coordinates and the projected rotational workspaces at each boundary position translated from neutral position ((a): $\mathbf{O}_k(20,20,140)$, (b): $\mathbf{O}_k(20,20,162.9)$).

Each range of the projected rotational workspaces is $39.3 \leq \Psi_B \leq 49.8^\circ$ and $58.5 \leq \Psi_P \leq 64.2^\circ$, where Ψ_B and Ψ_P are the tilt angles in the base and proposed models, respectively. The error ratio is $e = 37.7\%$, where $e = (((\Psi_{P,\max} - \Psi_{P,\min}) - (\Psi_{B,\max} - \Psi_{B,\min}))/(\psi_{B,\max} - \psi_{B,\min})) \times 100\%$. Also, Fig. 7 shows at each $\mathbf{O}_k$. Each range is $13.5 \leq \Psi_B \leq 25.8^\circ$ and $33.6 \leq \Psi_P \leq 46.5^\circ$, respectively. The error ratio is $e = 103.8\%$. The rotational workspace's volume of the proposed model is immensely wider than that of the base model on the boundary of the translational workspace. Consequently, from GCI, range of translational motion, tilt angle as well as the size of haptic device, all of the kinematic performance indices of the proposed model are better than those of the base model even though its size is slightly bigger than that of the base model. Especially, in the haptic device required large workspace for the sophisticated work, these results are much more useful.

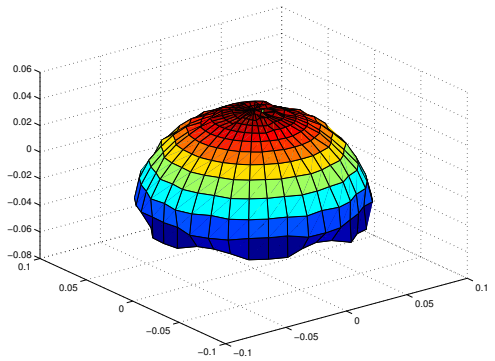

(a) Base model

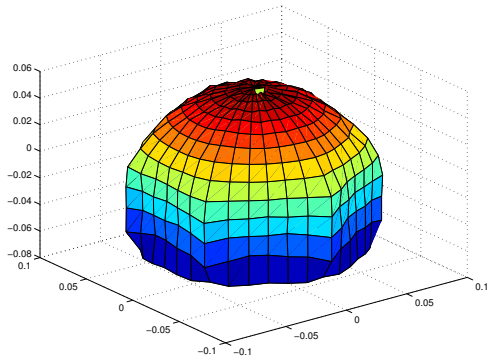

(b) Proposed model

Fig. 8. Comparison of translational workspaces at each neutral position of an end-effector: (a) $\mathbf{P}(0,0,120)$, (b) $\mathbf{P}(0,0,142.9)$ in Σ_b.

VI. Conclusions

In the development of mechanism like haptic device, the researcher should be taken into account multi degrees of freedom for the various works, compactness for easy transportation and control, lower cost, good performance index for quality of work, and easy installation, so on. However, it is important that how to combine and control them, since these design variables have the reciprocal relationship with each other. From this viewpoint, this paper presented the optimal design method of the 6-DOF haptic device with pantograph mechanism for the task required the large workspace. The method focused on that the haptic device takes the large rotational workspace throughout the entire translational workspace.

In optimization process, an objective function was composed of three kinematic performance indices: translational workspace, rotational workspace and GCI, and then it was maximized by the synthesis of them by a genetic algorithm to obtain the design linkage parameters for fifteen cases which are divided by the combination of given translational and rotational workspaces. As a result, we can obtain the best model improved all of the kinematic performances. The proposed method is very useful for development of device to use the work. In terms of identification and generalization, furthermore, the accurate criterion of qualitative and quantitative evaluation of results between the numerical model and the constructing model will be along the future topic.

References

[1] L. J. Stocco, S. E. Salcudean, and F. Sassani, "Optimal kinematic design of a haptic pen," *IEEE/ASME Transactions on Mechatronics*, vol. 6, no. 3, 2001, pp. 210–220.

[2] X. Kong and C. Gosselin, "Kinemtics and singularity analysis of a novel type of 3-CRR 3-DOF translational parallel manipulator," *The International Journal of Robotics Research*, vol. 21, no. 9, 2002, pp. 791–798.

[3] K. Vlachos and E. Papadopoulos, "Design and implement of a haptic device for training in urological operations," *IEEE Transactions on Robotics and Automation*, vol. 19, no. 5, 2003, pp. 801–809.

[4] J. Merlet, C. Gosselin, and N. Mouly, "Workspaces of planar parallel manipulator," *Mechanism and Machine Theory*, vol. 33, no. 1/2, 1998, pp.7–20.

[5] F. Bulca, J. Angeles, and P. J. Zsombor-Murray, "On the workspace determnation of spherical serial and platform mechanisms," *Mechanism and Machine Theory*, vol. 34, 1999, pp. 497–512.

[6] A. Kosinska, M. Galicki, and K. Kedzior, "Designing and optimization of parameters of delta-4 parallel manipulator for a given workspace," *Journal of Robotic Systems*, vol. 20, no. 9, 2003, pp. 539–548.

[7] M. Arsenault and R. Boudreau, "The synthesis of three-degree-of-freedom planar parallel mechanisms with revolute joints (3-RRR) for an optimal singularity-free workspace," *Journal of Robotic Systems*, vol. 21, no. 5, 2004, pp. 259–274.

[8] J. Yoon and J. Ryu, "Design, fabrication, and evaluation of a new haptic device using a parallel mechanism," *IEEE/ASME Transactions on Mechatronics*, vol. 6, no. 3, 2001, pp. 221–233.

[9] J. H. Holland, Adaptation in natural and artificial systems, The University of Michigan Press, Michigan, 1975.

[10] M. Mitchell, *An introduction to genetic algorithm*, Massachusetts Institute of Technology, 1996.

[11] I. A. Bonev and J. Ryu, "A new approach to orientation workspace analysis of 6-DOF parallel manipulators," *Mechanism and Machine Theory*, vol. 36, 2001, pp. 15–28.